Applied Surface Science 613 (2023) 156054

Contents lists available at ScienceDirect

Applied Surface Science

journal homepage: www.elsevier.com/locate/apsusc

Full Length Article

Computational studies of Ag_5 atomic quantum clusters deposited on anatase and rutile TiO_2 surfaces

Moteb Alotaibi [a,b], Qingqing Wu [a,*], Colin Lambert [a,*]

[a] Physics Department, Lancaster University, Lancaster LA1 4YB, United Kingdom
[b] Physics Department, Prince Sattam Bin Abdulaziz University, Alkharj 16278, Saudi Arabia

ARTICLE INFO

Keywords:
Atomic quantum clusters
Semiconductors
Geometrical stability
Electronic states
Photo absorption
Photo catalysis

ABSTRACT

Aiming at boosting the photocatalytic activities of rutile and anatase TiO_2 surfaces, an in-depth investigation of stoichiometric and reduced rutile TiO_2 (1 1 0) and anatase TiO_2 (1 0 1) decorated with bipyramidal and trapezoidal Ag_5 atomic quantum clusters (AQCs) is carried out. In this study, density functional theory (DFT) plus a Hubbard correction (U) is implemented to explore the geometric and electronic properties of such systems. It is found that the silver AQCs donate electrons to both stoichiometric and reduced TiO_2 surfaces resulting in the formation of a single polaron at either a fivefold coordinated (Ti_{5c}) atom or a sixfold coordinated (Ti_{6c}) atom, indicating improved surface activity. Depositing Ag_5 AQCs on both TiO_2 surfaces can produce mid-gap states within the band gap of the bulk, thereby improving the optical response of the composite in the visible and infrared. As expected, the number of mid-gap energy states increases further by introducing a single oxygen vacancy into the studied surfaces, which means that Ag_5 AQCs and oxygen vacancies can reinforce each other, leading to higher efficient photocatalytic activity. We also find that upon adsorption of Ag_5 AQCs on an anatase TiO_2 (1 0 1) surface, the energy required to form an oxygen vacancy is lower than that of rutile TiO_2 (1 1 0). Moreover, the adsorption of both bipyramidal and trapezoidal Ag_5 AQCs on both TiO_2 surfaces generally leads to significant distortion of the clusters, which accounts for the significant reduction in the total energy as compared to the pristine TiO_2. This detailed investigation provides insight into new mechanisms for enhancing photocatalytic efficiency of both rutile TiO_2 (1 1 0) and anatase TiO_2 (1 0 1) surfaces.

1. Introduction

Titania (TiO_2, titanium dioxide) has attracted considerable attention from scientists and engineers due to its high chemical and thermal stability, non-toxicity and relatively low cost [1–3]. These facts make it usable in multiple applications, such as solar cells [4], catalyst supports [5], waste-water treatment [6], water splitting [7–10], biomedication [11], micro-organism inactivation (such as viruses and bacteria) [12], reduction of carbon dioxide [13] and batteries [14]. TiO_2 has various polymorphs that naturally crystallise as well as some of which could be synthetically produced [15]. Rutile and anatase are the most abundant natural polymorphs [16,17]. However, the following drawbacks hinder their application in the photocatalytic activities [18]. First, the band gap energy (E_g) is approximately ~ 3.2 eV [19,20], which only allows the absorption of ultraviolet light (UV) (~4% of the solar radiation energy) and severely limits the response to visible light (~50 % of the solar radiation energy). Second, TiO_2 exhibits a large percentage of charge recombination of the photo-generated electrons and holes, which lowers down the photocatalytic process.

In order to overcome the above-mentioned disadvantages and improve the photocatalytic activities, numerous techniques have been implemented, such as combining other semiconductor materials with TiO_2 [21,22], dye sensitisation in photovoltaic cells [23], doping with metal [24] and non-metallic ions [25], and the deposition of noble metals [26]. It has been proved that depositing micro- and nanoparticles consisting of noble metals, such as palladium (Pd), platinum (Pt), gold (Au) and silver (Ag) as cocatalysts on TiO_2 surfaces can considerably enhance photocatalytic activities [27–34]. For example, Rusinque et al. [35] used a sol–gel approach to fabricate mesoporous TiO_2 decorated with Pd to study photocatalytic performance. Among the different amounts of doped Pd cocatalysts (i.e. 0.25–5 wt%), 0.25 wt% Pd@TiO_2 yielded the highest activity in the presence of ethanol as a hole scavenger under the visible light. Yu et al. [36] synthesised Pt fabricated on TiO_2 nanosheets with exposed (0 0 1) facets using a simple hydrothermal

* Corresponding authors.
E-mail addresses: q.wu6@lancaster.ac.uk (Q. Wu), c.lambert@lancaster.ac.uk (C. Lambert).

https://doi.org/10.1016/j.apsusc.2022.156054
Received 25 September 2022; Received in revised form 30 November 2022; Accepted 9 December 2022
Available online 13 December 2022

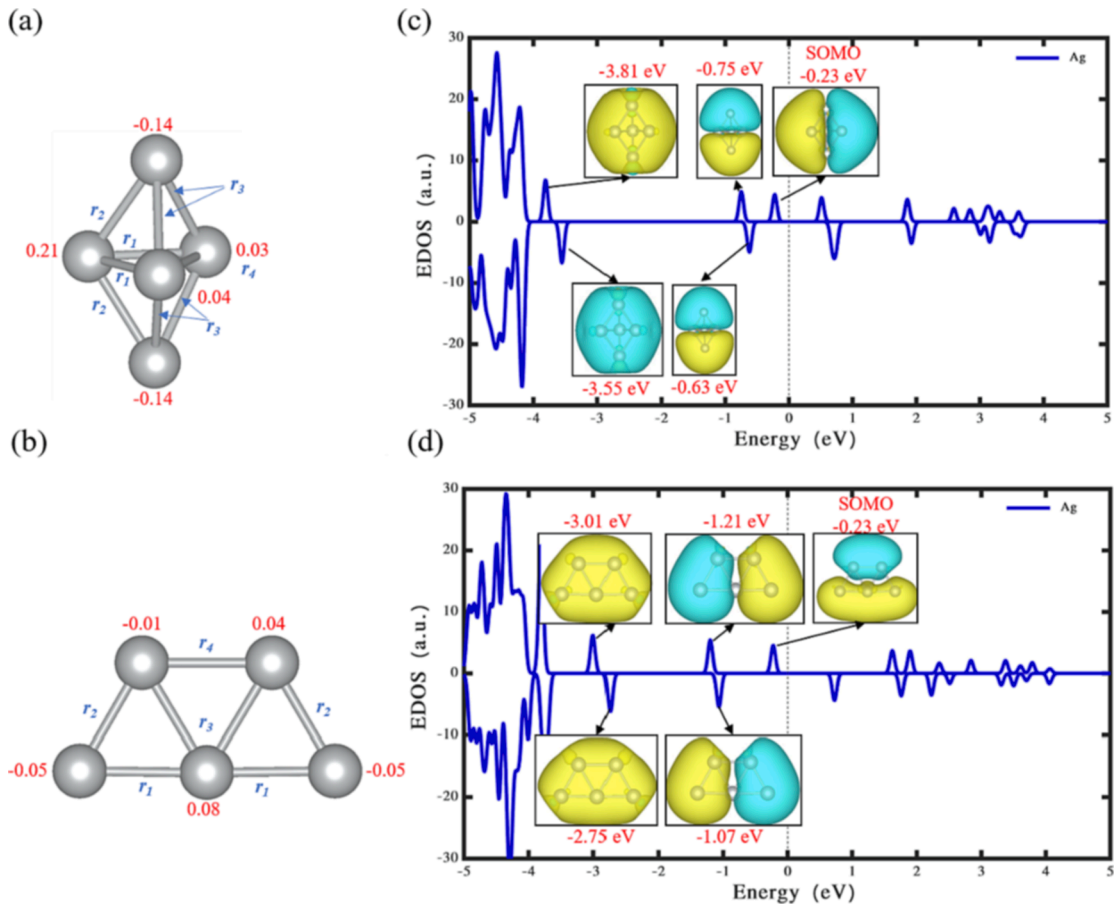

Fig. 1. Bipyramidal (a) and trapezoidal (b) Ag_5 isomers in the gas phase. Red numbers represent the net Bader charge distribution on each atom. r_1-r_4 show the Ag-Ag bond lengths. The corresponding values are shown in Table 1. (c) Density of states and frontier molecular orbitals of bipyramidal Ag_5. (d) Density of states and frontier molecular orbitals of trapezoidal Ag_5. SOMO: singly occupied molecular orbital. The yellow and blue reference colours of isosurfaces represent the positive and negative phases of wave functions (Note: the same reference colours are defined for all the wavefunction plots in subsequent figures.) and the isosurface value is 3.42×10^{-9} (a.u.). The vertical dashed line represents the Fermi energy level, which is set at a reference energy of 0 eV. (For interpretation of the references to colour in this figure legend, the reader is referred to the web version of this article.)

Table 1
Bond lengths of bipyramidal and trapezoidal Ag_5 isomers obtained using the hybrid functional HSE06.

Bond length (Å)	Bipyramidal Ag_5	Trapezoidal Ag_5
r_1	2.67	2.68
r_2	2.75	2.69
r_3	2.80	2.75
r_4	3.04	2.73

process. In their study, an ethanol solution was used as a sacrificial reagent for trapping holes. It was found that loading with 2 wt% of Pt nanoparticles exhibited the highest photocatalytic performance, and this can be attributed to the efficient charge separation caused by loading Pt nanoparticles.

A more recent study was conducted by Gogoi et al. [37]. In their study, a simple chemical reaction technique was implemented for synthesising an Ag-modified TiO_2 photocatalyst. It was found that among different amounts of Ag deposited on TiO_2, 1.5Ag@TiO_2 yielded the highest photoactivity for hydrogen generation in the presence of sacrificial agents (i.e. a mixture of Na_2SO_3, Na_2S and ethanol). This could be explained by the presence of oxygen vacancies, efficient charge separation and surface plasmonic resonance (SPR) resulting in minimisation of the band gap energy. Another recent work was reported by Ren et al. [38]. In their work, density functional theory (DFT) was employed to systematically study the influence of deposited 4d transition metals (TM) on photocatalytic activities of an anatase TiO_2 (1 0 1) surface. It was concluded that among the different studied 4d TM atoms, the deposition of both Ag and yttrium (Y) can effectively enhance the visible-light response of anatase TiO_2 (1 0 1) surface.

Lopez-Caballero et al. [39] theoretically studied the effect of the small Ag_5 atomic quantum clusters (AQCs) on perfect and reduced rutile TiO_2 (1 1 0) surfaces and the mechanism of improved photocatalytic activity via first-principles modelling. It was predicted that Ag_5 AQCs induce the formation of surface polarons by donating unpaired electrons to TiO_2, which tailor the band gap of titania and therefore, boosts its photocatalytic activity. These studies demonstrate that Ag_5 atomic clusters on both perfect and reduced rutile TiO_2 (1 1 0) surfaces improve the optical response of the substrate by enlarging its absorption range toward the visible light region. Moreover, Lopez-Caballero et al. [32] carried out X-ray absorption spectroscopy (XAS) and diffuse reflectance spectroscopy (DRS) measurements to investigate the properties of Ag_5@TiO_2. These were accompanied by DFT calculations of their electronic and optical properties. It was pointed out that photogenerated large polarons are formed at the interface of Ag_5-modified TiO_2. Their results also indicated that Ag_5@TiO_2 are visible-light photo-active materials and show potential for CO_2 reduction.

Even though extensive studies have been experimentally and theoretically conducted, the essential mechanisms required to design higher of levels photocatalytic materials are still not fully investigated. Importantly, for anatase titania, which has higher mobility for charge carriers, longer electron-hole pair life time and is more active than rutile

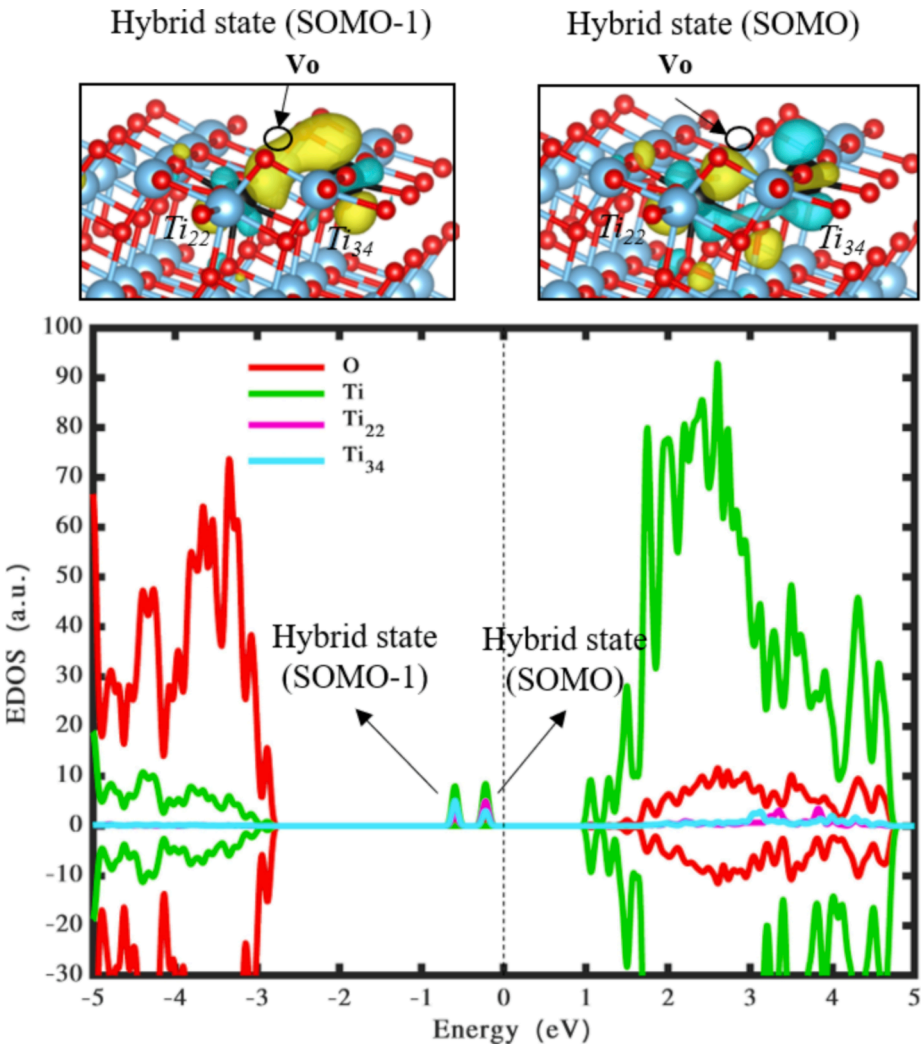

Fig. 2. Wavefunction and density of states of reduced anatase TiO_2 (1 0 1) surface. The green, red and blue show the states located on titanium, oxygen and silver atoms, while the pink and cyan peaks between −1–0 eV represent the polaronic states located on titanium atoms. SOMO-1: the second singly occupied molecular orbital and the isosurface value is 9.59×10^{-9} (a.u.). The vertical dashed line represents the Fermi energy level which is set at 0 eV. (For interpretation of the references to colour in this figure legend, the reader is referred to the web version of this article.)

for certain chemical reactions [40], the corresponding calculations are lacking in literature. Furthermore, an investigation of the photocatalytic performance of Ag_5 AQCs is particularly timely, because they can now be synthesized in bulk [41,42]. Therefore, these materials are becoming technologically relevant and it is important to carry out reliable calculations of their fundamental properties, in particular using the hybrid functional HSE06 for calculations of band structures and density of states. In this paper, DFT is used to understand the geometrical stabilities and the corresponding electronic structures that underpin the functioning of photocatalytic materials. Here, we investigate the doping effects of Ag_5 AQCs on the surfaces of stoichiometric and reduced anatase TiO_2 (1 0 1) and rutile TiO_2 (1 1 0). It is found that both Ag_5 AQCs and oxygen vacancies are able to change the photocatalytic activity of both TiO_2 surfaces by forming mid-gap states within the band gap of titania, which could allow the $Ag_5@TiO_{2-x}$ system to absorb longer wavelength photons than the pristine TiO_2. It is also found that the Ag_5 AQCs are easily adsorbed on the stoichiometric rutile TiO_2 (1 1 0) surface, compared with the anatase TiO_2 (1 0 1) surface, as demonstrated by their relative adsorption energies. In contrast, the formation energy of oxygen vacancy for Ag_5@ anatase TiO_{2-x} complex is lower than that of Ag_5@ rutile TiO_{2-x} complex.

2. Computational techniques

In order to simulate the electronic energy levels and charge densities of Ag_5 clusters and understand their ability to absorb photons, optimised geometries and electronic structures of Ag_5 AQCs and Ag_5/TiO_2 are obtained by implementing the hybrid exchange–correlation functional HSE06 with periodic boundary condition via Vienna initio Simulation Package (VASP 5.4.4) [43–46]. In the HSE06, the exchange correlation functional involves a short-range and long-range components of the Perdew-Burke-Ernzerhof (PBE) exchange functional, a short-range HF exchange and a PBE correlation functional [47]. To describe the interaction between valence electrons and the ion core, the projector augmented wave (PAW) method [48,49] and PAW-PBE [50,51] pseudopotentials are employed. The Ti (3 s, 4 s, 3p, 3d), O (2 s, 2p), and Ag (4d, 5 s) atomic orbitals are explicitly treated as valence electrons. Due to the self-interaction error resulting in artificial electron delocalization in the standard DFT methodologies, the generalised-gradient approximation (GGA) plus Hubbard term (U-term) is employed, in order to predict the accurate polaronic states [52] and band gap values of TiO_2. The U value implemented to titanium (3d) orbital in this work is 4.2 eV, which was originally reported in the literature [53–55].

The stoichiometric rutile TiO_2 (1 1 0) surface is modelled by building 12.04 Å x 13.12 Å unit cells containing four O-Ti-O trilayers ($Ti_{64}O_{128}$) with a 20 Å vacuum layer on top of the surface. The stoichiometric anatase TiO_2 (1 0 1) surface is modelled by 10.37 Å x 15.38 Å unit cells containing three O-Ti-O trilayers ($Ti_{48}O_{96}$) with a 19 Å vacuum layer on top of the surface. Large supercells of ($30 \times 30 \times 30$ Å^3) are used for isolated bare Ag_5 AQCs to ensure that no interaction takes place between the supercell and its periodic images. A k-point mesh was sampled, based on the Monkhorst-Pack scheme [56,57], in which all the

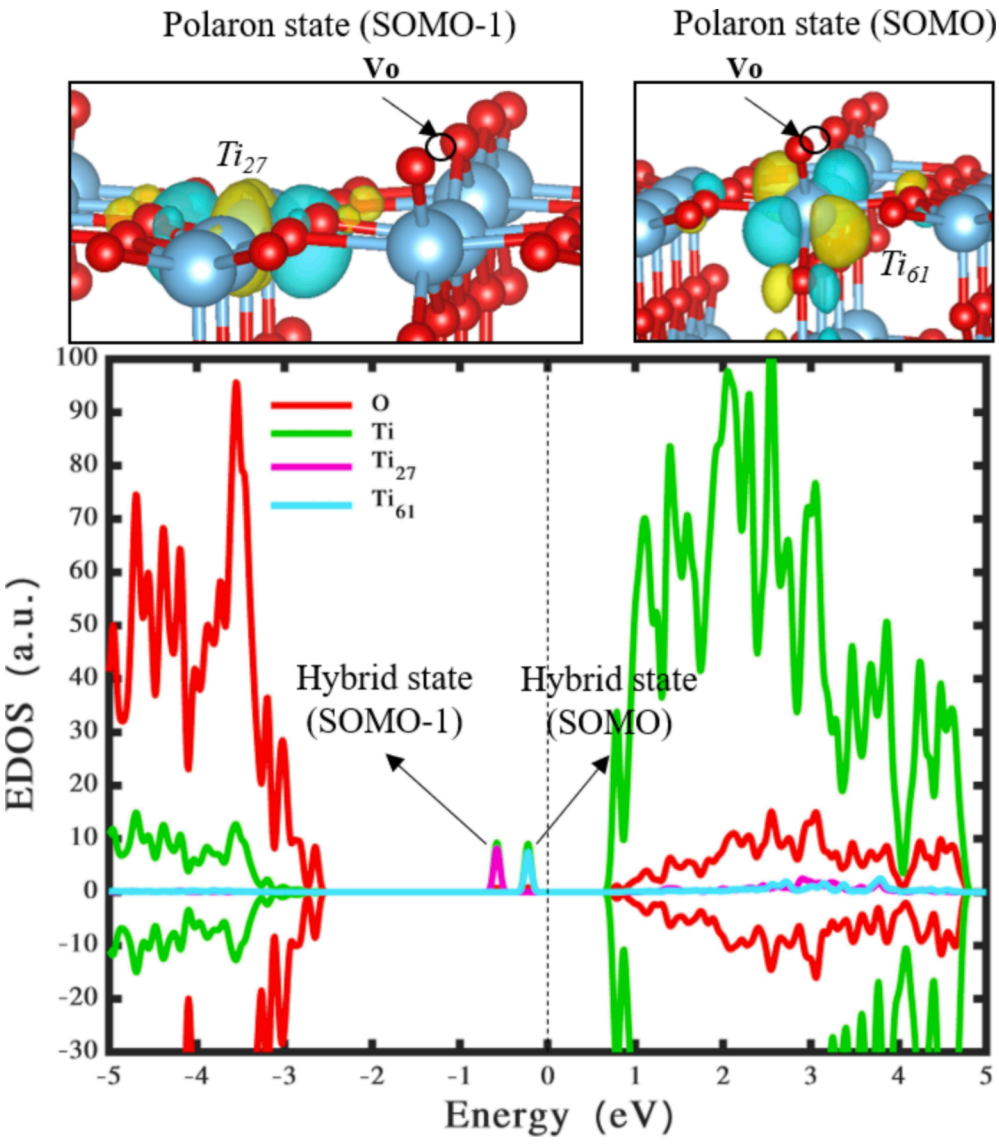

Fig. 3. Wavefunction and density of states of reduced rutile TiO_2 (1 1 0) surface. The green, red and blue show the states located on titanium, oxygen and silver atoms, while the pink and cyan peaks between −0.6–0 eV represent the polaronic states located on titanium atoms. The isosurface value is 9.83×10^{-8} (a.u.). The vertical dashed line represents the Fermi energy level which is set at 0 eV. (For interpretation of the references to colour in this figure legend, the reader is referred to the web version of this article.)

simulations are made using a single value of k-point. The cut-off energy for the planewaves basis set is fixed to 500 eV. A Gaussian smearing value of 0.05 eV is used for the band occupation due to the large supercell used in the tetrahedron. For the self-consistent electronic minimisation, a convergence threshold value of 10^{-4} eV is employed, and all modelled structures are allowed to relax with a threshold force value of 0.02 eV/Å.

The spin-polarised PBE combined with the Becke-Jonson (BJ) damping function in Grimmme's technique [58] is carried out in order in include van der Waals (vdW) corrections due its ability to predict accurate adsorption and binding energies of metal oxides materials [59]. In particular, Antonio et al. [60] included the vdW forces at different levels (DFT + D2, DFT + D2′, and vdW-DF method) to study the role of dispersion forces on Au, Ag single atoms and Au4, Ag4 clusters on TiO_2 and ZrO_2 (1 0 1) surfaces. It was found that the inclusion of vdW interactions can modify the order of stability of various isomers and lead to significant corrections to the adsorption energies. Furthermore, the adsorption properties will impact the diffusion and reaction properties of the adsorbates on AQC/oxide surfaces. Lara-Castells et al. [33] also used the vdW-corrected DFT-D3 technique to investigate the interaction energies of Ag clusters on a rutile TiO_2 (1 1 0) surface. It was pointed out that the vdW term also plays a key role, increasing rapidly the binding energies. Further tests, with and without vdW for Ag_5/anatase TiO_2 are carried out in the SI and agree well with literature. (See Fig. S8 of SI for more details). Therefore, the electronic structures of rutile TiO_2 (1 1 0), anatase TiO_2 (1 0 1) surfaces and Ag_5 deposited on both stoichiometric/reduced surfaces are carried out with spin-polarised HSE06 calculations based on the relaxed structures in the earlier DFT-D3 (BJ) calculations. The stability of the catalysts during chemical reactions is one of the most critical problems for practical utilisations. Therefore, the adsorption energy of Ag_5 cluster, E_{ads}, is computed to evaluate the adsorption stability based on the following formula,

$$E_{ads} = E_{total} - E_{slab} - E_m$$

where E_{total} is the total energy of slab and adsorbate in the same cell, E_{slab} is the total energy of the slab and E_m is the total energy of the isolated bare Ag_5 cluster. From the definition of adsorption energy, a negative value represents stable adsorption. When considering the presence of defects, the formation energy of an oxygen vacancy, E_{V_o}, can be calculated using the following formula,

$$E_{V_o} = E_{surface+V_o} - \frac{1}{2}E_{O_2} - E_{surface}$$

where $E_{Surface+V_O}$ is the total energy of the reduced/defective slab, E_{O_2} is the total energy of free oxygen in gas phase and $E_{Surface}$ is the total energy of the perfect/stoichiometric slab. It is worth mentioning that

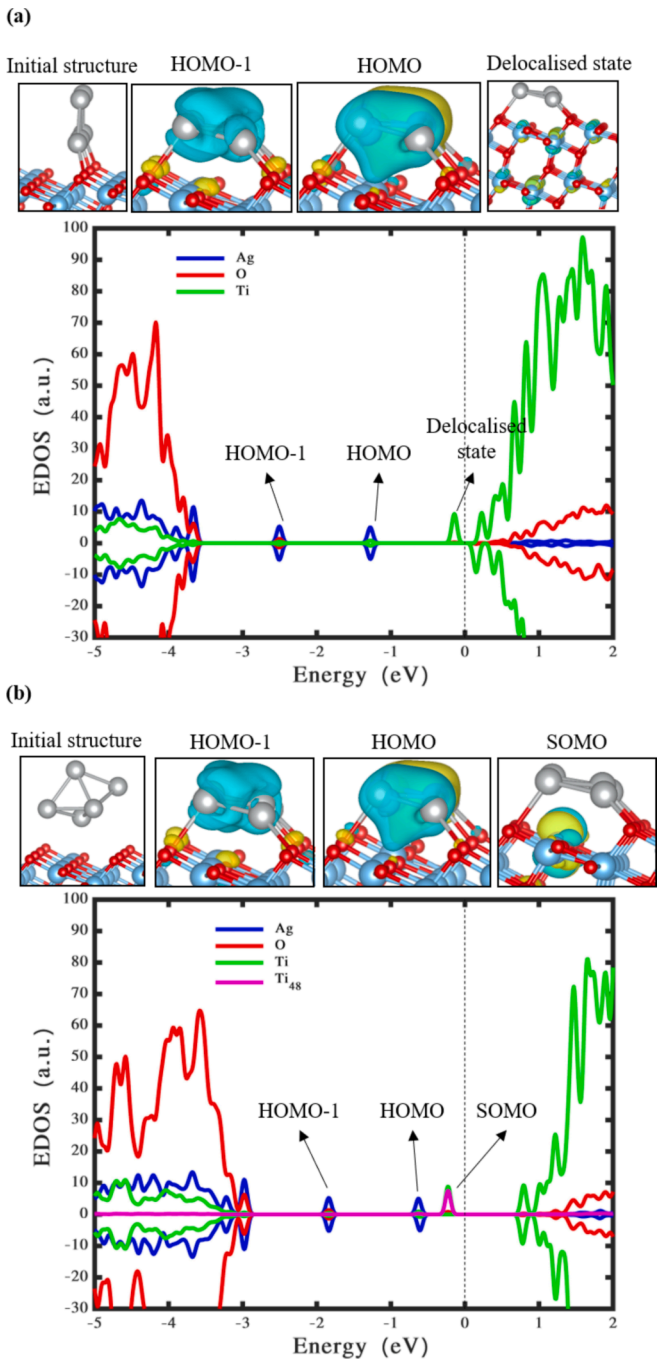

Fig. 4. Wavefunction and density of states of trapezoidal (a) and bipyramidal (b) Ag_5 clusters deposited on anatase TiO_2 (1 0 1) surface. The green, red and blue show the states located on titanium, oxygen and silver atoms, while the pink peak between −1–0 eV represents the polaronic states located on a titanium atom. The isosurface value of (a) is 8.00×10^{-8} (a.u.), and (b) is 8.00×10^{-9} (a.u.). The vertical dashed line represents the Fermi energy level which is set at 0 eV. (For interpretation of the references to colour in this figure legend, the reader is referred to the web version of this article.)

both adsorption and formation energies are evaluated at the GGA + U levels. All the presented structures are constructed and visualised using VESTA software [61].

3. Results and discussions

3.1. Geometrical and electronic properties of Ag_5 cluster

The optimised structures of both bipyramidal and trapezoidal Ag_5 AQCs in the gas phase are presented in Fig. 1(a) and (b). Both structures shown in Fig. 1 are obtained for the doublet state. These calculations reveal that in the gas phase, the trapezoidal shape (Fig. 1(b)) is more stable than the bipyramidal shape (Fig. 1(a)) by 0.49 eV in energy. The bipyramidal Ag_5 cluster shown in Fig. 1(b) is not precisely of D3h symmetry and is composed of equatorial Ag atoms (a triangular ring) with axial Ag atoms (top sites) above and below the ring. The three equatorial atoms are not all equivalent, since the three bonds shaping the triangle i.e., r_1 are equal to 2.67 Å, whereas the remaining bond i.e., r_4 is 3.04 Å. The bonds r_2 and r_3 formed by axial Ag with the three equatorial sites are equal to 2.69 Å and 2.75 Å respectively (see details in Table 1). The single unpaired electron of the Ag_5 (doublet with S = ½) (see Fig. 1(c)) is mainly situated on the two axial Ag atoms, and is similar to the charge distribution of Cu_5 [62] and Cu_7 cluster [63].

An unrestricted spin scheme utilising VASP.5.4.4 was implemented to appropriately treat the spin-polarisation of Ag_5 clusters. The bipyramidal configuration has energy gaps of 0.95 eV and 1.35 eV for spin up and spin down, respectively, which are smaller than those of trapezoidal Ag_5 (spin up: 1.85 eV, spin down: 1.8 eV). The singly occupied molecular orbital (SOMO)-lowest unoccupied molecular orbital (LUMO) gaps of both structures were also estimated (0.95 eV for bipyramidal and 1.85 eV for trapezoidal configurations) from the DOS figures (see Fig. 1(c) and (d)).

After the investigation of isolated Ag_5, in order to gain further insights into the geometrical stability and electronic states when Ag_5 AQCs are deposited on TiO_2 surfaces, we first simulated the pristine TiO_2 (Fig. S1 of SI) as benchmark. Specifically, a four-layer slab of rutile TiO_2 (1 1 0) and a three-layer slab of anatase TiO_2 (1 0 1) were constructed as shown in Fig. S1. As expected, the projected density of states presented in the right panels in Fig. S1 reveal that the valence band is mainly dominated by O (2p) orbitals, whereas the conduction band is mainly associated with Ti (3d) orbitals. The calculated band gap using the hybrid functional for rutile TiO_2 (1 1 0) is approximately 3.2 eV, which is in good agreement with experiment [19] and with previous DFT studies [64]. For anatase TiO_2 (1 0 1) this is around 3.6 eV, which is close to measured values [20,65]. Starting from these structures, defective (Fig. 2 and Fig. 3) TiO_2 surfaces are studies in section 3.2 and simulations of AQCs on these different surfaces are presented in sections 3.3 and 3.4.

3.2. Oxygen vacancies at surface and subsurface sites of anatase TiO_2 (1 0 1) and rutile TiO_2 (1 1 0)

3.2.1. Reduced anatase TiO_2 (1 0 1)

As a benchmark test, the simulations of the relative energetics of surface and subsurface oxygen vacancies are carried out. According to the results obtained for the different oxygen vacancy sites i.e., surface and subsurface (see Fig. S2 of the SI), it is found that the lowest formation energy is 4.26 eV when a twofold coordinated oxygen atom (O_{2c}) is removed from the top layer of the slab as shown in Fig. 2. While the formation energy of an oxygen vacancy in the sublayer of the slab is a 0.43 eV higher in energy (see Fig. S2 of the SI). Our findings are in good agreement with DFT + U calculations for a higher U values i.e., > 3.5 eV conducted by Cheng and Selloni [66].

Cheng and Selloni [66] studied the formation energy of oxygen vacancy on an anatase TiO_2 (1 0 1) surface as a function the U value and found that the formation energy is extremely sensitive to the choice of U. In particular, the formation energy of the sublayer is higher than the top layer when U lies between 3.5 and 4.5 eV, whereas the formation energy of the top layer becomes higher as compared to the sublayer, when the U value ranges between 2.5 eV and 3.0 eV. To illustrate the electronic

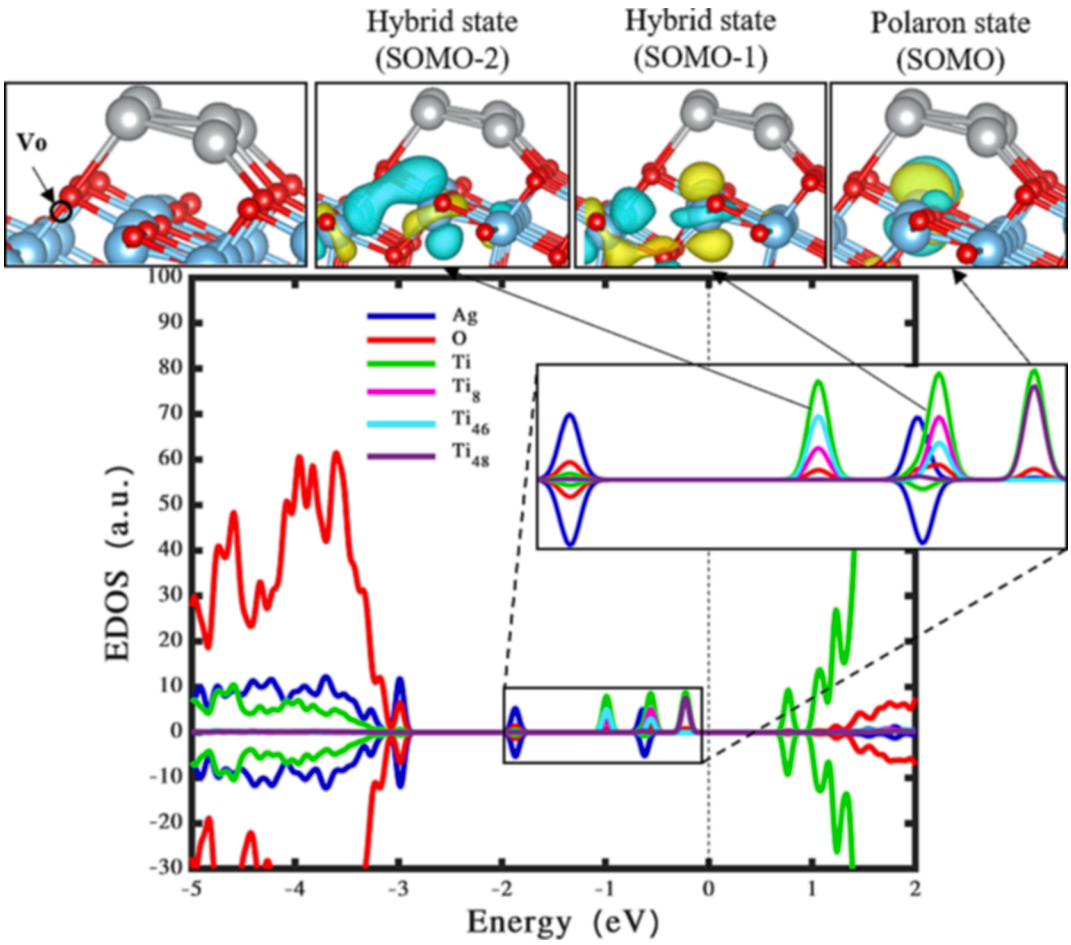

Fig. 5. Wavefunction and density of states of trapezoidal (a), tilted trapezoidal (b) and bipyramidal (c) Ag_5 clusters deposited on rutile TiO_2 (1 1 0) surface. The green, red and blue show the states located on titanium, oxygen and silver atoms, while the pink peaks between −1–0 eV represent the polaronic states located on a titanium atom. SOMO-2: the third singly occupied molecular orbital. The isosurface value is 4.61×10^{-8} (a.u.). The vertical dashed line represents the Fermi energy level which is set at 0 eV. (For interpretation of the references to colour in this figure legend, the reader is referred to the web version of this article.)

structures of the reduced anatase TiO_2 (1 0 1) surface, Fig. 2 shows its optimised configuration. Two excess electrons localise at a fivefold coordinated titanium atom (Ti_{5c}) and a sixfold coordinated titanium atom (Ti_{6c}) creating polaronic states (pink peak at −0.23 eV and cyan peak at −0.60 eV) which are 1.16 eV and 1.53 eV below the conduction band edge, respectively.

3.2.2. *Reduced rutile TiO_2 (1 1 0)*

To compare the results with the reduced anatase TiO_2 (1 0 1) surface, we investigated the relative energetics of the top layer and sublayer oxygen vacancies of rutile TiO_2 (1 1 0) surface, which are extensively investigated both experimentally and theoretically. Our DFT + U calculations are carried out for an O_{2c} vacancy at the top layer of the slab (see Fig. 3) using a U value of 4.2 eV [53–55]. At the DFT-GGA level, the formation energies of oxygen vacancies at the top layer of the slab (see Fig. 3) are lower than those at the sublayer (see Fig. S3 of the SI) approximately by 0.6 eV, which is in good agreement with previous theoretical calculations [66–69].

In all studied cases, the O_{2c} vacancy in the top layer creates two polaronic states localised at two Ti_{5c} in the top layer of the slab (see Fig. 3). As shown in the density of states in Fig. 3, the oxygen vacancy energy levels lie at 0.87 and 1.22 eV below the bottom of the conduction band. The energies of these gap states are in excellent agreement with electron energy loss spectroscopy (EELS) measurements [70]. To conclude, the formation of oxygen vacancy of the bridging oxygen (O_{2c}) at the top layer of the slab is favoured for rutile TiO_2 (1 1 0) surface.

3.3. *The deposition of trapezoidal and bipyramidal Ag_5 on anatase TiO_2(1 0 1)*

3.3.1. *On pristine anatase TiO_2(1 0 1)*

Trapezoidal (see Fig. 4a) and bipyramidal (see Fig. 4b) Ag_5 clusters are deposited on anatase TiO_2 (1 0 1) surface with the corresponding wavefunctions as shown in Fig. 4. After geometrical optimisation, both silver clusters relax to a lying-down trapezoidal Ag_5, which is completely attached to the substrate surface. The trapezoidal Ag_5 cluster transfers 0.91 e^- to Ti atoms, creating a delocalised state located just at the bottom of the conduction band edge. This higher energy level state is active and could play a key role in photo-catalytical processes. In order to confirm this delocalised state, we performed a DFT + U calculation using a value of U = 2.5 eV (see Fig. S4 in the SI document). Similarly, the bipyramidal Ag_5 cluster transfers 0.89 e^- to a Ti^{+3} (3d) in the surface of anatase TiO_2 (1 0 1) leading to the formation of a polaron at 0.9 eV below the conduction band edge (see the pink peak at −0.23 eV). The polaronic state can be clearly seen by the wavefunction SOMO in Fig. 4, which is located just underneath the silver cluster. To characterize the polaron state in the bipyramidal case, we analysed the Ti-O bond lengths for the Ti atom, in the vicinity of the polaron, as shown in Fig. S9 and Table S1. It is found that the bonds are elongated compared to the normal Ti-O bonds in the absence of a polaron. The adsorption energy of Ag_5 cluster for the former is −2.88 eV and for the latter is −3.54 eV.

The highest occupied molecular orbital (HOMO) of the Ag_5 cluster on an anatase TiO_2 (1 0 1) surface mixes stronger with Ti^{+3} (3d) states than

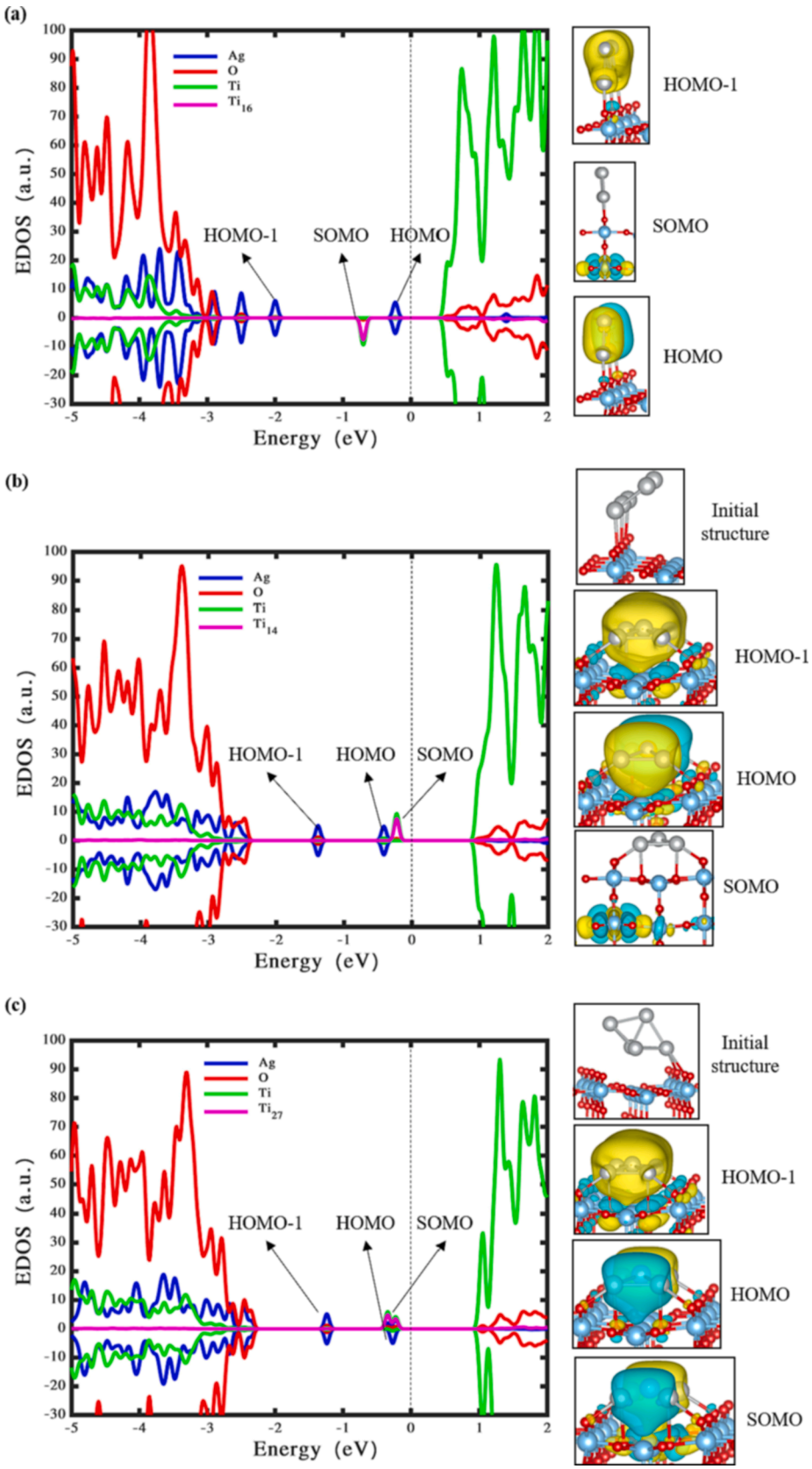

Fig. 6. Wavefunction and density of states of trapezoidal (a), tilted trapezoidal (b) and bipyramidal (c) Ag_5 clusters deposited on rutile TiO_2 (1 1 0) surface. The green, red and blue show the states located on titanium, oxygen and silver atoms, while the pink peaks between −1–0 eV represent the polaronic states located on a titanium atom. The isosurface value is 4.61×10^{-8} (a.u.). The vertical dashed line represents the Fermi energy level which is set at 0 eV. (For interpretation of the references to colour in this figure legend, the reader is referred to the web version of this article.)

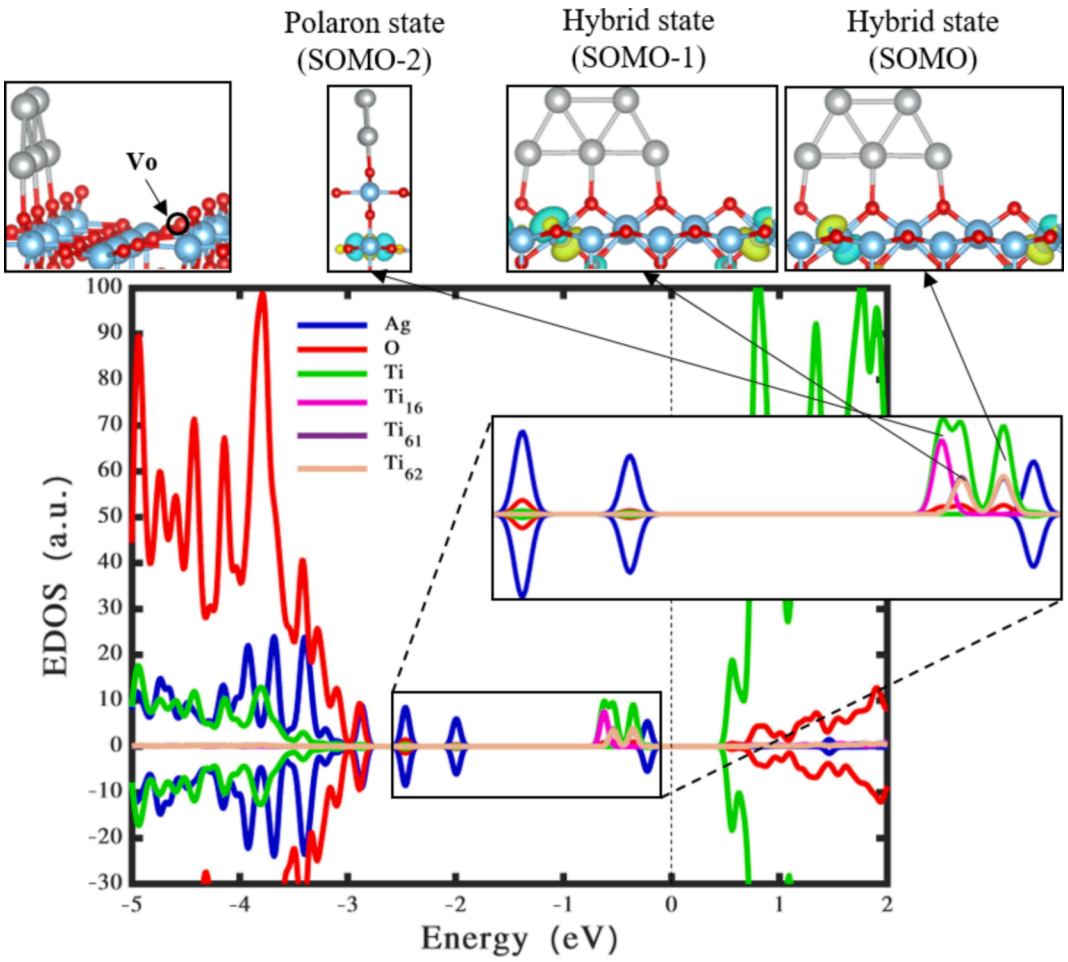

Fig. 7. Wavefunction and density of states of trapezoidal Ag_5 deposited on reduced rutile TiO_2 (1 1 0) surface. The green, red and blue show the states located on titanium, oxygen and silver atoms, while the pink, brown and purple peaks between −1–0 eV represent the polaronic states located on titanium atoms. The isosurface value is 1.00×10^{-7} (a.u.). The vertical dashed line represents the Fermi energy level which is set at 0 eV. (For interpretation of the references to colour in this figure legend, the reader is referred to the web version of this article.)

the bridging oxygen atoms at −1.23 eV for the trapezoidal shape and at −0.63 eV for the bipyramidal shape. In contrast, the overlap of the second highest occupied molecular orbital (HOMO-1) of the Ag_5 cluster is stronger with O (2p) states of the bridging oxygen atoms than that the Ti^{+3} (3d) states at −2.6 eV for the trapezoidal shape and at −1.84 eV for the bipyramidal shape. Furthermore, fewer gap states are found in the mid-gap range between −3.0 eV and 0 eV unlike the gap states formed by a Cu_5 cluster reported in a previous DFT study [62]. These gap states can improve the photocatalytic efficiency of rutile and anatase TiO_2 material [71]. Based on the projected density of states, the Ag_5 cluster becomes nonmagnetic after donating an electron, while the support gains the electron and becomes paramagnetic with one unpaired electron (see Fig. 4b). This phenomenon was also observed for a Cu_5 cluster when deposited on a rutile TiO_2 (1 1 0) surface [62].

3.3.2. *On reduced anatase TiO_2 (1 0 1)*

Having analysed the electronic structure of Ag_5 clusters deposited on a pristine anatase TiO_2 (1 0 1) surface in the ground electronic state, we further investigated the electronic structure of Ag_5 clusters deposited on a reduced anatase TiO_2 (1 0 1) surface. Upon adsorption of an Ag_5 cluster, Ag_5 and an oxygen vacancy are able to induce three surface polarons demonstrated in Fig. 5. The trapezoidal Ag_5 cluster transfers 0.87 e^- to anatase TiO_2 (1 0 1) surface, which is a 0.02 e^- lower charge transfer than the stoichiometric anatase TiO_2 (1 0 1) surface. The formation energy of an oxygen vacancy in anatase Ag_5-TiO_2 (1 0 1) is 4.31 eV, which slightly increases by a factor of 0.05 eV as compared to the pristine anatase TiO_2 (1 0 1). Thus, it is concluded that the deposition of the Ag_5 cluster on anatase TiO_2 (1 0 1) does not affect the process in which an oxygen vacancy can occur. Further optimal configurations using different sites of oxygen vacancy can be found in Fig. S5.

3.4. *The deposition of trapezoidal and bipyramidal Ag_5 on rutile TiO_2(1 1 0)*

3.4.1. *On pristine rutile TiO_2 (1 1 0)*

Three adsorption configurations of Ag_5 clusters deposited on the rutile TiO_2 (1 1 0) surface are evaluated: the upstanding trapezoidal, tilted trapezoidal and bipyramidal Ag_5 clusters. The corresponding density of states and most relevant frontier molecular are shown in Fig. 6. From Fig. 6a, we can see that the trapezoidal shape of Ag_5 persists. However, when the trapezoidal Ag_5 cluster is tilted towards the TiO_2 surface (see Fig. 6b), it is drastically deformed to a new planar shape, which is more stable compared to the upstanding configuration by a 1.24 eV lower energy. In contrast, as clearly seen in Fig. 6c, upon adsorption, the bipyramidal Ag_5 cluster is deformed to a new pyramidal configuration, which becomes the most stable structure differing by a 1.81 eV compared to the up-standing trapezoidal Ag_5 (see Fig. 6a).

As depicted in the projected density of states in Fig. 6, one polaron state forming the singly occupied molecular orbital (referred to as SOMO) is located on a Ti^{3+} (3d) in the sublayer of the substrate for the trapezoidal configurations and located on a Ti^{3+} (3d) in the top layer of the substrate for the bipyramidal configuration (represented by the pink

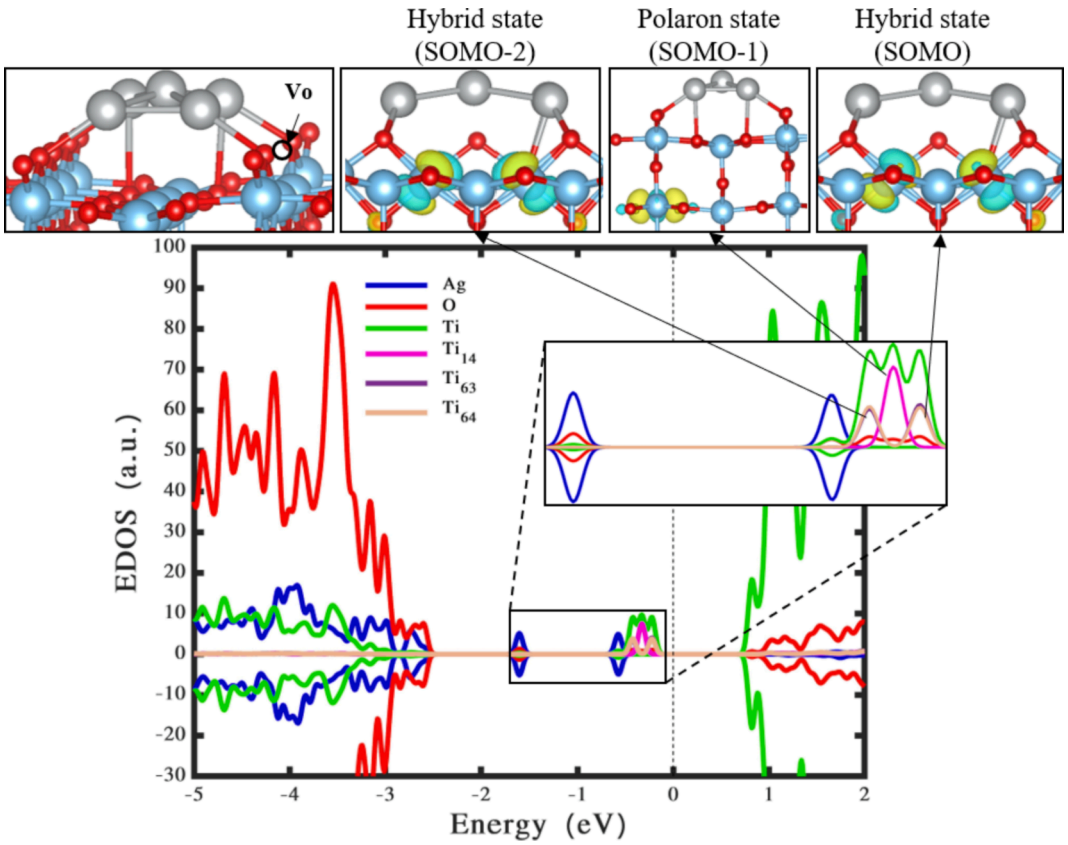

Fig. 8. Wavefunction and density of states of new planar Ag_5 deposited on reduced rutile TiO_2 (1 1 0) surface. The green, red and blue show the states located on titanium, oxygen and silver atoms, while the pink, brown and purple peaks between −1–0 eV represent the polaronic states located on titanium atoms. The isosurface value is 1.00×10^{-7} (a.u.). The vertical dashed line represents the Fermi energy level which is set at 0 eV. (For interpretation of the references to colour in this figure legend, the reader is referred to the web version of this article.)

peaks next to the wavefunction SOMO in Fig. 6). Owing to the fact that the states formed by silver align mainly with the valence band, the existence of the polaronic state is crucial for absorbing photons in the visible light region [72]. Based on Bader charge analysis, the trapezoidal Ag_5 clusters shown in Fig. 6a and b are positively charged and transfer about 0.74 e^- and 0.94 e^- to the substrate, respectively. Additionally, the bipyramidal Ag_5 cluster presented in Fig. 6c is positively charged and donates approximately 0.89 e^- to the substrate creating the polaron at −0.3 eV, which is approximately 1.2 eV below the edge of the conduction band. The same value was obtained by Di Valentin et al for a Ti_{5c} (3d) state in reduced and hydroxylated rutile TiO_2 (1 1 0) [73].

3.4.2. *On reduced rutile TiO_2 (1 1 0)*

Based upon the optimised configurations illustrated in Fig. 6, we now study the effect of the presence of one oxygen vacancy. A similar trend to the reduced anatase TiO_2 (1 0 1) surface is observed for the reduced rutile TiO_2 (1 1 0) where both Ag_5 and an oxygen vacancy are able to induce three surface polarons as can be seen in Fig. 7 and Fig. 8. The deposition of an Ag_5 cluster and the presence of an oxygen vacancy reinforce each other and lead to the formation of three polaronic states, in which one is formed due to the charge transfer from Ag_5 cluster to the support and the other two are formed due to the presence of the oxygen vacancy for both cases. In particular, in the corresponding projected density of states, the localised Ti^{+3} (3d) orbitals (occupying the SOMOs) lie between 0.78 eV and 1.03 eV below the conduction band edge for the upstanding trapezoidal shape and between 0.92 eV and 1.13 eV below the conduction band edge for the new planar shape. These states will affect the dynamics of the photogenerated charges [74] as well as decelerating the electron-hole pairs recombination resulting in improved catalytic activity.

In addition, it is found that the amount of charge transfer from the Ag_5 cluster to the support is slightly less, as compared to the stoichiometric rutile TiO_2 (1 1 0) surface (see Fig. 6a). For example, the upstanding trapezoidal Ag_5 cluster donates 0.73 e^- to the reduced rutile TiO_2 (1 1 0) surface, which is a 0.01 e^- less charge transfer than the stoichiometric surface (see Fig. 6a). The new planar Ag_5 cluster (shown in Fig. 8) donates 0.85 e^- to the reduced rutile TiO_2 (1 1 0) surface, which is a 0.04 e^- less than the stoichiometric surface (see Fig. 6c). This could be attributed to the presence of the oxygen vacancy, where the charge distributes to a less extent than on defective TiO_2 surfaces [39]. The formation energy of an oxygen vacancy in reduced rutile Ag_5-TiO_2 (1 1 0) is 4.44 eV for the upstanding configuration (see Fig. 7) and is 4.47 eV for the new planar configuration (see Fig. 8). It is worth mentioning that upon the deposition of the Ag_5 cluster on reduced rutile TiO_2 (1 1 0), the formation energy of oxygen vacancy in the case of the up-standing configuration increases approximately 0.38 eV and in the case of the new planar configuration raises 0.41 eV as compared to pristine rutile TiO_2 (1 1 0). Further optimal configurations using different sites of oxygen vacancy can be found in Fig. S6 and Fig. S7.

4. Conclusion

We have studied the stability of trapezoidal and bipyramidal Ag_5 AQCs in the gas phase and demonstrated that the trapezoidal Ag_5 AQC is more stable than the bipyramidal Ag_5 AQC. We have also systematically studied the electronic structures of Ag_5 AQCs deposited on both anatase TiO_2 (1 0 1) and rutile TiO_2 (1 1 0) surfaces, with and without the presence of an oxygen vacancy and have shown that mid-gap states are formed due to the adsorption of Ag_5 AQCs and the presence of oxygen vacancies. Both the trapezoidal and bipyramidal Ag_5 AQCs create only

one polaronic state in both TiO_2 surfaces either on the top layer or on the first sublayer. Two more polaronic states are created, when introducing an oxygen vacancy into Ag_5@TiO_2 complex of both surfaces. Importantly, the polarons and other gap states persist, which reveals that Ag_5 and oxygen vacancies can reinforce each other. Moreover, the creation of an oxygen vacancy requires less energy for the Ag_5@ anatase TiO_2 (1 0 1) complex as compared to the Ag_5@ rutile TiO_2 (1 1 0) complex. Distortion of Ag_5 AQCs have been clearly demonstrated when adsorbed on both TiO_2 surfaces. Upon surface adsorption, both bipyramidal and trapezoidal Ag_5 AQCs are oxidised, donating their electrons to the substrates of all the modelled structures. The highest net charge is correlated with the highest adsorption energies obtained. It has also been demonstrated that deposited Ag_5 AQCs and the created oxygen vacancy on photocatalyst surface of both titania surfaces can efficiently separate the electron-hole pairs and therefore, could enhance their photocatalytic activity. The theoretical findings presented in this study shed light on new strategies for improving the photocatalytic efficiency of such systems.

CRediT authorship contribution statement

Moteb Alotaibi: Investigation, Methodology, Writing – original draft. **Qingqing Wu:** Supervision, Writing – review & editing. **Colin Lambert:** Supervision, Writing – review & editing.

Declaration of Competing Interest

The authors declare that they have no known competing financial interests or personal relationships that could have appeared to influence the work reported in this paper.

Data availability

Data will be made available on request.

Appendix A. Supplementary material

Supplementary data to this article can be found online at https://doi.org/10.1016/j.apsusc.2022.156054.

References

[1] C. Kim, M. Choi, J. Jang, Nitrogen-doped SiO2/TiO2 core/shell nanoparticles as highly efficient visible light photocatalyst, Catal. Commun. 11 (5) (2010) 378–382, https://doi.org/10.1016/j.catcom.2009.11.005.

[2] A. Murphy, P. Barnes, L. Randeniya, I. Plumb, I. Grey, M. Horne, J. Glasscock, Efficiency of solar water splitting using semiconductor electrodes, Int. J. Hydrogen Energy 31 (14) (2006) 1999–2017.

[3] F. Akira, T.N. Rao, D.A. Tryk, Titanium dioxide photocatalysis, J. Photochem. Photobiol. C 1 (1) (2000) 1–21.

[4] X. He, Y. Guo, J. Liu, X. Li, J. Qi, Fabrication of peanut-like TiO2 microarchitecture with enhanced surface light trapping and high specific surface area for high-efficiency dye sensitized solar cells, J. Power Sources 423 (January) (2019) 236–245, https://doi.org/10.1016/j.jpowsour.2019.03.090.

[5] Y. Maeda, Y. Iizuka, M. Kohyama, Generation of oxygen vacancies at a Au/TiO2 perimeter interface during co oxidation detected by in situ electrical conductance measurement, J. Am. Chem. Soc. 135 (2) (2013) 906–909, https://doi.org/10.1021/ja310999c.

[6] M.S. Hamdy, W.H. Saputera, E.J. Groenen, G. Mul, A novel TiO2 composite for photocatalytic wastewater treatment, J. Catal. 310 (2014) 75–83, https://doi.org/10.1016/j.jcat.2013.07.017.

[7] J. Wu, S. Lu, D. Ge, L. Zhang, W. Chen, H. Gu, Photocatalytic properties of Pd/TiO2 nanosheets for hydrogen evolution from water splitting, RSC Adv. 6 (72) (2016) 67502–67508, https://doi.org/10.1039/c6ra10408h.

[8] S. Kment, F. Riboni, S. Pausova, L. Wang, L. Wang, H. Han, Z. Hubicka, J. Krysa, P. Schmuki, R. Zboril, Photoanodes based on TiO2 and α-Fe2O3 for solar water splitting-superior role of 1D nanoarchitectures and of combined heterostructures, Chem. Soc. Rev. 46 (12) (2017) 3716–3769.

[9] X. Chen, S.S. Mao, Titanium dioxide nanomaterials: synthesis, properties, modifications and applications, Chem. Rev. 107 (7) (2007) 2891–2959, https://doi.org/10.1021/cr0500535.

[10] F. De Angelis, C. Di Valentin, S. Fantacci, A. Vittadini, A. Selloni, Theoretical studies on anatase and less common TiO2phases: bulk, surfaces, and nanomaterials, Chem. Rev. 114 (19) (2014) 9708–9753, https://doi.org/10.1021/cr500055q.

[11] Z. Fei Yin, L. Wu, H. Gui Yang, Y. Hua Su, Recent progress in biomedical applications of titanium dioxide, Phys. Chem. Chem. Phys. 15 (14) (2013) 4844–4858, https://doi.org/10.1039/c3cp43938k.

[12] M. Kralova, P. Dzik, M. Vesely, J. Cihlar, Preparation and characterization of doped titanium dioxide printed layers, Catal. Today 230 (2014) 188–196, https://doi.org/10.1016/j.cattod.2013.09.018.

[13] L. Wei, C. Yu, Q. Zhang, H. Liu, Y. Wang, TiO2-based heterojunction photocatalysts for photocatalytic reduction of CO2 into solar fuels, J. Mater. Chem. A 6 (45) (2018) 22411–22436, https://doi.org/10.1039/c8ta08879a.

[14] G.N. Zhu, Y.G. Wang, Y.Y. Xia, Ti-based compounds as anode materials for Li-ion batteries, Energy Environ. Sci. 5 (5) (2012) 6652–6667, https://doi.org/10.1039/c2ee03410g.

[15] T. Zhu, S.P. Gao, The stability, electronic structure, and optical property of tio 2 polymorphs, J. Phys. Chem. C 118 (21) (2014) 11385–11396, https://doi.org/10.1021/jp412462m.

[16] D.A. Panayotov, J.R. Morris, Surface chemistry of Au/TiO2: thermally and photolytically activated reactions, Surf. Sci. Rep. 71 (1) (2016) 77–271, https://doi.org/10.1016/j.surfrep.2016.01.002.

[17] Ş. Neaţu, J.A. Maciá-Agulló, P. Concepción, H. Garcia, Gold-copper nanoalloys supported on TiO2 as photocatalysts for CO2 reduction by water, J. Am. Chem. Soc. 136 (45) (2014) 15969–15976.

[18] M. Ni, M.K.H. Leung, D.Y.C. Leung, K. Sumathy, A review and recent developments in photocatalytic water-splitting using TiO2 for hydrogen production, Renew. Sustain. Energy Rev. 11 (3) (2007) 401–425, https://doi.org/10.1016/j.rser.2005.01.009.

[19] Y. Tezuka, S. Shin, T. Ishii, T. Ejima, S. Suzuki, S. Sato, Photoemission and Bremsstrahlung Isochromat spectroscopy studies of Ti02 (Rutile) and SrTi03, J. Phys. Soc. Jpn. 63 (1) (1994) 347–357, https://doi.org/10.1143/JPSJ.63.347.

[20] L. Kavan, M. Grätzel, S.E. Gilbert, C. Klemenz, H.J. Scheel, Electrochemical and photoelectrochemical investigation of single-crystal anatase, J. Am. Chem. Soc. 118 (28) (1996) 6716–6723, https://doi.org/10.1021/ja954172l.

[21] S. Chainarong, L. Sikong, S. Pavasupree, S. Niyomwas, Synthesis and characterization of nitrogen-doped TiO2 nanomaterials for photocatalytic activities under visible light, Energy Procedia 9 (2011) 418–427, https://doi.org/10.1016/j.egypro.2011.09.046.

[22] H. Fujii, K. Inata, M. Ohtaki, K. Eguchi, H. Arai, Synthesis of TiO2/CdS nanocomposite via TiO2 coating on CdS nanoparticles by compartmentalized hydrolysis of Ti alkoxide, J. Mater. Sci. 36 (2) (2001) 527–532, https://doi.org/10.1023/A:1004857419242.

[23] M. Mba, M. D'Acunzo, P. Salice, T. Carofiglio, M. Maggini, S. Caramori, A. Campana, A. Aliprandi, R. Argazzi, S. Carli, C.A. Bignozzi, Sensitization of nanocrystalline TiO2 with multibranched organic dyes and co(III)/(II) Mediators: strategies to improve charge collection efficiency, J. Phys. Chem. C 117 (39) (2013) 19885–19896.

[24] M. Klein, J. Nadolna, A. Gołąbiewska, P. Mazierski, T. Klimczuk, H. Remita, A. Zaleska-Medynska, The effect of metal cluster deposition route on structure and photocatalytic activity of mono- and bimetallic nanoparticles supported on TiO 2 by radiolytic method, Appl. Surf. Sci. 378 (2016) 37–48.

[25] H. Zhang, H. Ming, S. Lian, H. Huang, H. Li, L. Zhang, Y. Liu, Z. Kang, S.-T. Lee, Fe2O3/carbon quantum dots complex photocatalysts and their enhanced photocatalytic activity under visible light, Dalt. Trans. 40 (41) (2011) 10822, https://doi.org/10.1039/c1dt11147g.

[26] C.-H. Liang, M.-F. Hou, S.-G. Zhou, F.-B. Li, C.-S. Liu, T.-X. Liu, Y.-X. Gao, X.-G. Wang, J.-L. Lü, The effect of erbium on the adsorption and photodegradation of orange I in aqueous Er3+-TiO2 suspension, J. Hazard. Mater. 138 (3) (2006) 471–478.

[27] C. Su, C.H. Liao, J. Di Wang, C.M. Chiu, B.J. Chen, The adsorption and reactions of methyl iodide on powdered Ag/TiO 2, Catal. Today 97 (1 SPEC. ISS) (2004) 71–79, https://doi.org/10.1016/j.cattod.2004.04.053.

[28] W. Grünert, A. Brückner, H. Hofmeister, P. Claus, Structural properties of Ag/TiO2 catalysts for acrolein hydrogenation, J. Phys. Chem. B 108 (18) (2004) 5709–5717, https://doi.org/10.1021/jp049855e.

[29] H. Tran, J. Scott, K. Chiang, R. Amal, Clarifying the role of silver deposits on titania for the photocatalytic mineralisation of organic compounds, J. Photochem. Photobiol. A Chem. 183 (1–2) (2006) 41–52, https://doi.org/10.1016/j.jphotochem.2006.02.018.

[30] M. Haruta, M. Daté, Advances in the catalysis of Au nanoparticles, Appl. Catal. A Gen. 222 (1–2) (2001) 427–437, https://doi.org/10.1016/S0926-860X(01)00847-X.

[31] A. Sclafani, J.M. Herrmann, Influence of metallic silver and of platinum-silver bimetallic deposits on the photocatalytic activity of titania (anatase and rutile) in organic and aqueous media, J. Photochem. Photobiol. A Chem. 113 (2) (1998) 181–188, https://doi.org/10.1016/S1010-6030(97)00319-5.

[32] P. López-Caballero, J.M. Ramallo-López, L.J. Giovanetti, D. Buceta, S. Miret-Artés, M.A. López-Quintela, F.G. Requejo, M.P. de Lara-Castells, Exploring the properties of Ag5-TiO2 interfaces: Stable surface polaron formation, UV-Vis optical response, and CO2 photoactivation, J. Mater. Chem. A 8 (14) (2020) 6842–6853.

[33] M.P. De Lara-Castells, C. Cabrillo, D.A. Micha, A.O. Mitrushchenkov, T. Vazhappilly, Ab initio design of light absorption through silver atomic cluster decoration of TiO2, Phys. Chem. Chem. Phys. 20 (28) (2018) 19110–19119, https://doi.org/10.1039/c8cp02853b.

[34] A.S. Mazheika, V.E. Matulis, O.A. Ivashkevich, Quantum chemical study of adsorption of Ag2, Ag4 and Ag8 on stoichiometric TiO2 (1 1 0) surface, J. Mol.

Struct. Theochem. 942 (1–3) (2010) 47–54, https://doi.org/10.1016/j.theochem.2009.11.032.
[35] B. Rusinque, S. Escobedo Salas, H. de Lasa, Photoreduction of a Pd-doped mesoporous TiO2 photocatalyst for hydrogen production under visible light, Catalysts 10 (1) (2020), doi: 10.3390/catal10010074.
[36] J. Yu, L. Qi, M. Jaroniec, Hydrogen production by photocatalytic water splitting over Pt/TiO 2 nanosheets with exposed (001) facets, J. Phys. Chem. C 114 (30) (2010) 13118–13125, https://doi.org/10.1021/jp104488b.
[37] D. Gogoi, A. Namdeo, A.K. Golder, N.R. Peela, Ag-doped TiO2 photocatalysts with effective charge transfer for highly efficient hydrogen production through water splitting, Int. J. Hydrogen Energy 45 (4) (2020) 2729–2744, https://doi.org/10.1016/j.ijhydene.2019.11.127.
[38] Y. Ren, et al., Effects of 4d transition metals doping on the photocatalytic activities of anatase TiO2 (101) surface, Int. J. Quantum Chem. 121 (16) (2021) 1–10, https://doi.org/10.1002/qua.26683.
[39] P. López-Caballero, S. Miret-Artés, A.O. Mitrushchenkov, M.P. de Lara-Castells, Ag 5 -induced stabilization of multiple surface polarons on perfect and reduced TiO 2 rutile (110), J. Chem. Phys. 153 (16) (2020) 164702.
[40] U. Diebold, N. Ruzycki, G.S. Herman, A. Selloni, One step towards bridging the materials gap: surface studies of TiO 2 anatase, Catal. Today 85 (2–4) (2003) 93–100, https://doi.org/10.1016/S0920-5861(03)00378-X.
[41] V. Porto, D. Buceta, B. Domínguez, C. Carneiro, E. Borrajo, M. Fraile, N. Davila-Ferreira, I.R. Arias, J.M. Blanco, M.C. Blanco, J.M. Devida, L.J. Giovanetti, F. G. Requejo, J.C. Hernández-Garrido, J.J. Calvino, M. López-Haro, G. Barone, A. M. James, T. García-Caballero, D.M. González-Castaño, M. Treder, W. Huber, A. Vidal, M.P. Murphy, M.A. López-Quintela, F. Domínguez, Silver clusters of five atoms as highly selective antitumoral agents through irreversible oxidation of thiols, Adv. Funct. Mater. 32 (29) (2022) 2113028.
[42] I.R. Arias, D. Buceta, G. Barone, M.C. Giménez-López, H. Lozano, M. Lazzari, M. Arturo López-Quintela, Ag5 nanoclusters with dual catalytic antiradical activities, J. Colloid Interface Sci. 628 (2022) 437–447.
[43] G. Kresse, J. Furthmüller, Efficiency of ab-initio total energy calculations for metals and semiconductors using a plane-wave basis set, Comput. Mater. Sci. 6 (1) (1996) 15–50, https://doi.org/10.1016/0927-0256(96)00008-0.
[44] G. Kresse, J. Furthmüller, Efficient iterative schemes for ab initio total-energy calculations using a plane-wave basis set, Phys. Rev. B 54 (1996) 11169–11186, https://doi.org/10.1021/acs.jpca.0c01375.
[45] G. Kresse, J. Hafner, Ab initio molecular-dynamics simulation of the liquid-metalamorphous- semiconductor transition in germanium, Phys. Rev. B 49 (20) (1994) 14251–14269, https://doi.org/10.1103/PhysRevB.49.14251.
[46] G. Kresse, J. Hafner, Ab initio molecular dynamics for liquid metals, Phys. Rev. B 47 (1) (1993) 558–561, https://doi.org/10.1103/PhysRevB.47.558.
[47] A.V. Krukau, O.A. Vydrov, A.F. Izmaylov, G.E. Scuseria, Influence of the exchange screening parameter on the performance of screened hybrid functionals, J. Chem. Phys. 125 (22) (2006) 224106.
[48] D. Kresse, D. Joubert, From ultrasoft pseudopotentials to the projector augmented-wave method, Phys. Rev. B 59 (3) (1999) 1758–1775, https://doi.org/10.1103/PhysRevB.59.1758.
[49] P.E. Blöchl, Projector augmented-wave method, Phys. Rev. B 50 (24) (1994) 17953–17979, https://doi.org/10.1103/PhysRevB.50.17953.
[50] J.P. Perdew, K. Burke, M. Ernzerhof, Generalized gradient approximation made simple, Phys. Rev. Lett. 77 (18) (1996) 3865–3868, https://doi.org/10.1103/PhysRevLett.77.3865.
[51] M.J. Gillan, D. Alfè, A. Michaelides, Perspective: How good is DFT for water? J. Chem. Phys. 144 (13) (2016) 1–33, https://doi.org/10.1063/1.4944633.
[52] N. Seriani, C. Pinilla, Y. Crespo, Presence of gap states at Cu/TiO2 anatase surfaces: consequences for the photocatalytic activity, J. Phys. Chem. C 119 (12) (2015) 6696–6702, https://doi.org/10.1021/acs.jpcc.5b00846.
[53] B.J. Morgan, G.W. Watson, A DFT + U description of oxygen vacancies at the TiO2 rutile (1 1 0) surface, Surf. Sci. 601 (21) (2007) 5034–5041, https://doi.org/10.1016/j.susc.2007.08.025.
[54] B.J. Morgan, G.W. Watson, A density functional theory + u study of Oxygen vacancy formation at the (110), (100), (101), and (001) surfaces of rutile TiO2, J. Phys. Chem. C 113 (17) (2009) 7322–7328, https://doi.org/10.1021/jp811288n.
[55] B.J. Morgan, G.W. Watson, Intrinsic n-type defect formation in TiO 2: a comparison of rutile and anatase from GGA+ U calculations, J. Phys. Chem. C 114 (2010) 2321–2328, https://doi.org/10.1021/jp301913c.
[56] H.J. Monkhorst, J.D. Pack, Special points for Brillonin-zone integrations, Phys. Rev. B 13 (1976) 5188–5192, https://doi.org/10.1039/c8ta11250a.
[57] J.D. Pack, H.J. Monkhorst, Special points for Brillonln-zone integrations"—a reply, Phys. Rev. 16 (4) (1977) 1748–1749.
[58] S. Grimme, J. Antony, S. Ehrlich, H. Krieg, A consistent and accurate ab initio parametrization of density functional dispersion correction (DFT-D) for the 94 elements H-Pu, J. Chem. Phys. 132 (15) (2010), 154104, https://doi.org/10.1063/1.3382344.
[59] A. Antony, C. Hakanoglu, A. Asthagiri, J.F. Weaver, Dispersion-corrected density functional theory calculations of the molecular binding of n-alkanes on Pd(111) and PdO(101), J. Chem. Phys. 136 (5) (2012), 054702, https://doi.org/10.1063/1.3679167.
[60] A.R. Puigdollers, P. Schlexer, G. Pacchioni, Gold and silver custers on TiO2 and ZrO2 (101) surfaces: Role of dispersion forces, J. Phys. Chem. C 119 (27) (2015) 15381–15389, https://doi.org/10.1021/acs.jpcc.5b04026.
[61] K. Momma, F. Izumi, VESTA 3 for three-dimensional visualization of crystal, volumetric and morphology data, J. Appl. Crystallogr. 44 (6) (2011) 1272–1276, https://doi.org/10.1107/S0021889811038970.
[62] Q. Wu, S. Hou, D. Buceta, H.J.L. Ordoñez, M. Arturo López-Quintela, C.J. Lambert, Tuning the surface states of TiO2 using Cu5 atomic clusters, Appl. Surf. Sci. 594 (2022), 153455, https://doi.org/10.1016/j.apsusc.2022.153455.
[63] J.H. Stenlid, A.J. Johansson, T. Brinck, Searching for the thermodynamic limit-a DFT study of the step-wise water oxidation of the bipyramidal Cu7 cluster, Phys. Chem. Chem. Phys. 16 (6) (2014) 2452–2464, https://doi.org/10.1039/c3cp53865f.
[64] A. Janotti, J.B. Varley, P. Rinke, N. Umezawa, G. Kresse, C.G. Van De Walle, Hybrid functional studies of the oxygen vacancy in TiO2, Phys. Rev. B - Condens. Matter Mater. Phys. 81 (8) (2010), 085212, https://doi.org/10.1103/PhysRevB.81.085212.
[65] H. Tang, F. Lévy, H. Berger, P.E. Schmid, Urbach tail of anatase TiO2, Phys. Rev. B 52 (11) (1995) 7771–7774, https://doi.org/10.1103/PhysRevB.52.7771.
[66] H. Cheng, A. Selloni, Energetics and diffusion of intrinsic surface and subsurface defects on anatase TiO2 (101), J. Chem. Phys. 131 (5) (2009), 054703, https://doi.org/10.1063/1.3194301.
[67] Y. He, O. Dulub, H. Cheng, A. Selloni, U. Diebold, Evidence for the predominance of subsurface defects on reduced anatase TiO2(101), Phys. Rev. Lett. 102 (10) (2009), 106105, https://doi.org/10.1103/PhysRevLett.102.106105.
[68] J. Oviedo, M.A.S. Miguel, J.F. Sanz, Oxygen vacancies on TiO2 (110) from first principles calculations, J. Chem. Phys. 121 (15) (2004) 7427–7433, https://doi.org/10.1063/1.1796253.
[69] T. Pabisiak, A. Kiejna, Energetics of oxygen vacancies at rutile TiO2(110) surface, Solid State Commun. 144 (7–8) (2007) 324–328, https://doi.org/10.1016/j.ssc.2007.08.043.
[70] M.A. Henderson, W.S. Epling, C.H.F. Peden, C.L. Perkins, Insights into photoexcited electron scavenging processes on TiO2 obtained from studies of the reaction of O2 with OH groups adsorbed at electronic defects on TiO2(110), J. Phys. Chem. B 107 (2) (2003) 534–545, https://doi.org/10.1021/jp0262113.
[71] A.B. Schvval, A. Juan, G.F. Cabeza, Theoretical study of the role of the interface of Ag4 nanoclusters deposited on TiO2(110) and TiO2(101), Appl. Surf. Sci. 490 (February) (2019) 343–351, https://doi.org/10.1016/j.apsusc.2019.05.291.
[72] E.C. Tyo, S. Vajda, Catalysis by clusters with precise numbers of atoms, Nat. Nanotechnol. 10 (7) (2015) 577–588, https://doi.org/10.1038/NNANO.2015.140.
[73] C. Di Valentin, G. Pacchioni, A. Selloni, Electronic structure of defect states in hydroxylated and reduced rutile TiO2(110) surfaces, Phys. Rev. Lett. 97 (16) (2006), 166803, https://doi.org/10.1103/PhysRevLett.97.166803.
[74] L. Liu, Y. Li, Understanding the reaction mechanism of photocatalytic reduction of CO2 with H2O on TiO2-based photocatalysts: a review, Aerosol Air Qual. Res. 14 (2) (2014) 453–469, https://doi.org/10.4209/aaqr.2013.06.0186.